Microstructure and Capacitance of the Electrical Double Layers at the Interface of Ionic Liquids and Planar Electrodes

G. Feng,[†] J. S. Zhang,[‡] and R. Qiao*,[†]

Department of Mechanical Engineering, Clemson University, Clemson, South Carolina 29634, and Department of Thermal Engineering, Tsinghua University, Beijing, China, 100084

Received: November 10, 2008; Revised Manuscript Received: December 25, 2008

We report on the molecular dynamics simulations of the electrical double layers (EDLs) at the interface of ionic liquids [BMIM][NO_3] and planar electrodes. Simulations confirm that a Helmholtz-like interfacial counterion layer exists when the electrode charge density is negative or strongly positive, but the counterion layer is not well-defined when the electrode charge density is weakly positive. The thickness of the EDL, as inferred from how deep the charge separation and orientational ordering of the ions penetrate into the bulk ILs, is about 1.1 nm. The liquid nature of the IL and the short-range ion−electrode and ion−ion interactions are found to significantly affect the structure of the EDL, particularly at low electrode charge densities. Charge delocalization of the ions is found to affect the mean force experienced by the ions and, thus, can play an important role in shaping the EDL structure. The differential capacitance of the EDLs is found to be nearly constant under negative electrode polarization but increases dramatically with the potential under positive electrode polarization. We show that the differential capacitance is a quantitative measure of the response of the EDL structure to a change in electrode charge density. It is found that the $[NO_3]^-$ ion dominates the response of EDL structure to the change in electrode charge under both positive and negative electrode polarization, which is qualitatively different from that in aqueous electrolytes. Detailed analysis shows that the cation−anion correlations and the strong adsorption of $[BMIM]^+$ ions on the electrode are responsible for the capacitance−potential correlation observed here.

I. Introduction

Room temperature ionic liquids (ILs) are a new class of electrolytes that have received significant attention in recent years due to many of their unique properties. ILs are composed *entirely* of ions but remain in the liquid state at room temperature.[1,2] Compared to other simpler electrolytes, such as aqueous electrolytes and high-temperature molten salts, the ions in ILs are bulkier and often feature a complex shape. In addition, their charges are typically delocalized among many atoms.[3] Most of the ILs have a very low vapor pressure and excellent thermal stability, and many of them have wide electrochemical windows.[1,2] These properties offer distinct advantages in many electrochemical applications, such as supercapacitors, solar cells, and batteries.[4−7] For example, when ILs are used as the working electrolyte in supercapacitors, their wide electrochemical window and excellent thermal stability help improve the energy density and reliability of the supercapacitor.[5] In this and other applications, the microstructure and capacitance of the electrical double layers (EDLs) at the interface of ILs and electrodes play an essential role in determining the system performance. Therefore, it is important to obtain a thorough understanding of these EDLs.

Given the solvent-free nature of the ILs and the complex shape of the ions in ILs, it is expected that the classical theories for the EDLs in dilute aqueous electrolytes and high-temperature molten salts cannot accurately describe the structure and properties of the EDLs at the interface of ILs and electrified surfaces.[8,9] The structure of these EDLs has been studied by experimental and analytical methods. Experimental data suggest that the IL−electrode interface is one ion layer thick (typically 3−5 Å), which supports the idea that the EDLs in ILs are essentially Helmholtz layers.[10] Surface frequency generation data indicate that the interfacial cations exhibit orientational ordering and their orientation depends not only on the electrical potential of the electrode but also on the type of anions in the ILs.[10,11] Recently, several elegant analytical models have been proposed to describe the EDLs in ILs.[8,9] It was hypothesized that the EDLs in ILs consist of a compact inner layer and a "diffusive" outer layer. Although these new models are still mean-field theories and focus on the role of long-range electrostatic interactions in determining the EDL structure, the solvent-free nature of the ILs is accounted for. The most extensively studied macroscopic property of the EDLs in ILs is their differential capacitance.[10,12−14] Two different types of trends have been reported. Whereas concave capacitance−electrode potential ($C-V$) curves were observed in many experiments,[10,13,14] bell-shaped and camel-like $C-V$ curves have also been reported.[12] Although none of the existing theories can rigorously explain these diverse and seemingly contradictory experimental observations, important progress has been made recently. For example, the bell-shaped and camel-like $C-V$ curves can be explained by the EDL models proposed by Kornyshev and Oldham,[8,9] although rigorous justification of the model parameter remains a challenge.[12]

Since the EDLs in ILs are truly molecular phenomena, atomistic simulations can be very helpful in elucidating their microstructure and macroscopic properties. However, systematic study of the EDLs near an electrified surface by using atomistic simulation is rare. In ref 15, the density and orientation of IL

* Corresponding author. E-mail: rqiao@ces.clemson.edu. URL: http://www.clemson.edu/~rqiao.
[†] Clemson University.
[‡] Tsinghua University.

10.1021/jp809900w CCC: $40.75
Published on Web 02/20/2009

ions near a structureless electrode with low surface charge density (±0.02 C/m^2) were studied by using molecular dynamics simulations. In this study, a Helmholtz layer-like counterion layer near charged electrodes, consistent with that inferred from experimental studies, was, indeed, observed. However, the orientational ordering of the cation persists at a position ~10Å from the electrode, which is far greater as compared to the EDL thickness inferred from experimental data.[10] In ref 16, the capacitance of a minimal-model IL was studied by molecular dynamics simulations, and a quasi-bell-like $C-V$ curve was observed, in qualitative agreement with some earlier experimental results.[12] Although the solvent-free nature of the IL and size asymmetry of the cations and anions are accounted for in this pioneering study, other important molecular details of the ILs (e.g., the complex shape and charge delocalization of the ions) are neglected.

In this work, we study the microstructure and capacitance of the EDLs at the interface of ILs and planar electrodes by modeling the electrode and ILs with full chemical details using a classical molecular dynamics (MD) method. Our simulations show that the EDL structure is affected not only by the "ionic" nature of the ILs, but also by the "liquid" nature of the ILs and the charge delocalization of ions. The concave-shaped $C-V$ curves reported in the literature are qualitatively reproduced in our simulations and can be traced to strong correlations between cation and anions and the significant adsorption of bulky cations on the electrode. The rest of the paper is organized as follows: the simulation method and MD models are presented in Section II; the results on the EDL microstructure and capacitance are discussed in Section III; and finally, conclusions are presented in Section IV.

II. Simulation Method and Models

We performed molecular dynamics simulations of [BMIM-][NO_3] liquids enclosed between two oppositely charged channel walls. Each wall was modeled as a slab of α-quartz oriented in the [100] direction. The channel width was set to 6.63 nm (measured between the innermost layers of the opposing channel walls) to produce a bulklike behavior in the channel center. The coordinate system was chosen such that the innermost layer of the lower channel wall corresponds to $z = 0$. A periodic boundary condition was applied in the directions parallel to the channel wall. No intrinsic partial charges were assigned on the channel wall atoms. Thirteen cases with surface charge densities (σ) ranging from 0.00, ±0.01 to ±0.12 C/m^2 were studied. To produce a given wall charge density, a small charge was added to the atoms in the innermost wall layers. The Lennard−Jones parameters for the channel wall atoms were taken from the Gromacs force field.[17] The force fields for the $[BMIM]^+$ and $[NO_3]^-$ ions were taken from ref 18.

Simulations were performed in the NVT ensemble using an MD package Gromacs.[19] The IL temperature was maintained by using a Berendsen thermostat with a time constant of 1.0 ps. The number of IL molecules inside the channel was adjusted so that the IL density in the channel center matched that of the bulk IL within 0.5% when the channel walls were electrically neutral. Although it is desirable that the IL density in the channel center remain constant for all the systems studied, it was found that the IL density at the channel center decreases by about 0.75% as the charge density of the channel wall increases from 0 to ±0.12 C/m^2. To evaluate the dependence of EDL observables on the IL density in the channel center, we performed additional simulations for the channel system with surface charge densities of ±0.10 C/m^2 by reducing/increasing the number of IL molecules in the system by 2.38%. The simulation results on the EDL structure and electrical potential inside EDL were found to vary only marginally as the number of IL molecules inside the system changed, thus indicating that the result obtained in this work is insensitive to the precise value of the IL density at the channel center. To compute the electrostatic interactions in the two-dimensionally periodic geometry adopted here, the slab-PME method was used. The dimension of the simulation box in the channel width direction was set to be 5 times the channel width,[20,21] which is sufficient to ensure that the accuracy of electrostatic force calculation is comparable to that of the two-dimensional Ewald method.[21] An FFT grid spacing of 0.12 nm and cubic interpolation for charge distribution were used to compute the electrostatic interactions in the reciprocal space. A cutoff distance of 1.0 nm was used in the calculation of electrostatic interactions in the real space. The nonelectrostatic interactions were computed by direct summation with a cutoff length of 1.0 nm. The shape of the $[BMIM]^+$ and $[NO_3]^-$ ions was maintained by using the LINCS algorithm.[22] For each simulation case, the MD system was first simulated at 1000 K for 3 ns, and the system temperature was quenched by 200 K at the end of the simulation. This procedure was repeated until the system temperature reached 400 K. After that, the system temperature was quenched to 360 K, and a 9 ns equilibration run was performed. This was followed by a 12−36-ns-long production run. To ensure the accuracy of the simulation results, each case was repeated five times with different initial configurations.

III. Results and Discussion

A. EDL Microstructure. ***Results.*** Figure 1a and b shows the number density of $[NO_3]^-$ and $[BMIM]^+$ ions near positively charged electrodes. Throughout this paper, the location of cations and anions are computed on the basis of the geometrical center of the imidazolium ring and the entire anion, respectively. Figure 1a indicates that as the surface charge density (σ) increases, the $[NO_3]^-$ ion density near the electrode increases dramatically, and the location of the first peak moves toward the electrode. At $\sigma = 0.09$ C/m^2, a single $[NO_3]^-$ ion layer can be clearly delineated in the region $z = 0.15-0.41$ nm, which seems to support the Helmholtz model for the EDL. However, the MD results also point to several new features unavailable in the Helmholtz model. First, a distinct Helmholtz layer is difficult to delineate at relatively low electrode charge densities; for example, $\sigma < 0.03$ C/m^2. Second, there is a significant accumulation of $[BMIM]^+$ ions within the first counterion layer, particularly at low surface charge densities. As σ increases, the $[BMIM]^+$ density peak becomes lower and moves away from the electrode, but a significant $[BMIM]^+$ ion accumulation can still be observed in the region $z = 0.27-0.45$ nm, even at $\sigma =$ 0.09 C/m^2 (see Figure 1b). Third, the thickness of the EDL is much larger than that of the first counterion layer. This is seen clearly from the space charge density profile near the electrode, as shown in Figure 1c, where charge separation is observed at s position as far as $z = 1.0$ nm from the electrode. Finally, ionic liquids exhibit a rich structure at positions much beyond the first counterion layer. For example, rather than being a constant, the density of the IL near a neutral electrode exhibits significant oscillation at a position as far as 1.0 nm from the electrode. The IL structure is also quantified by computing the order parameter of the ions $P_2(\cos\theta) = <(3\cos^2\theta - 1)/2>$, where θ is defined as the angle formed by the normal vector of the electrode and the normal vector of the imidazolium ring of the $[BMIM]^+$ ion or the plane formed by the three oxygen atoms of the $[NO_3]^-$ ion. Figure 1d and e shows the distribution of

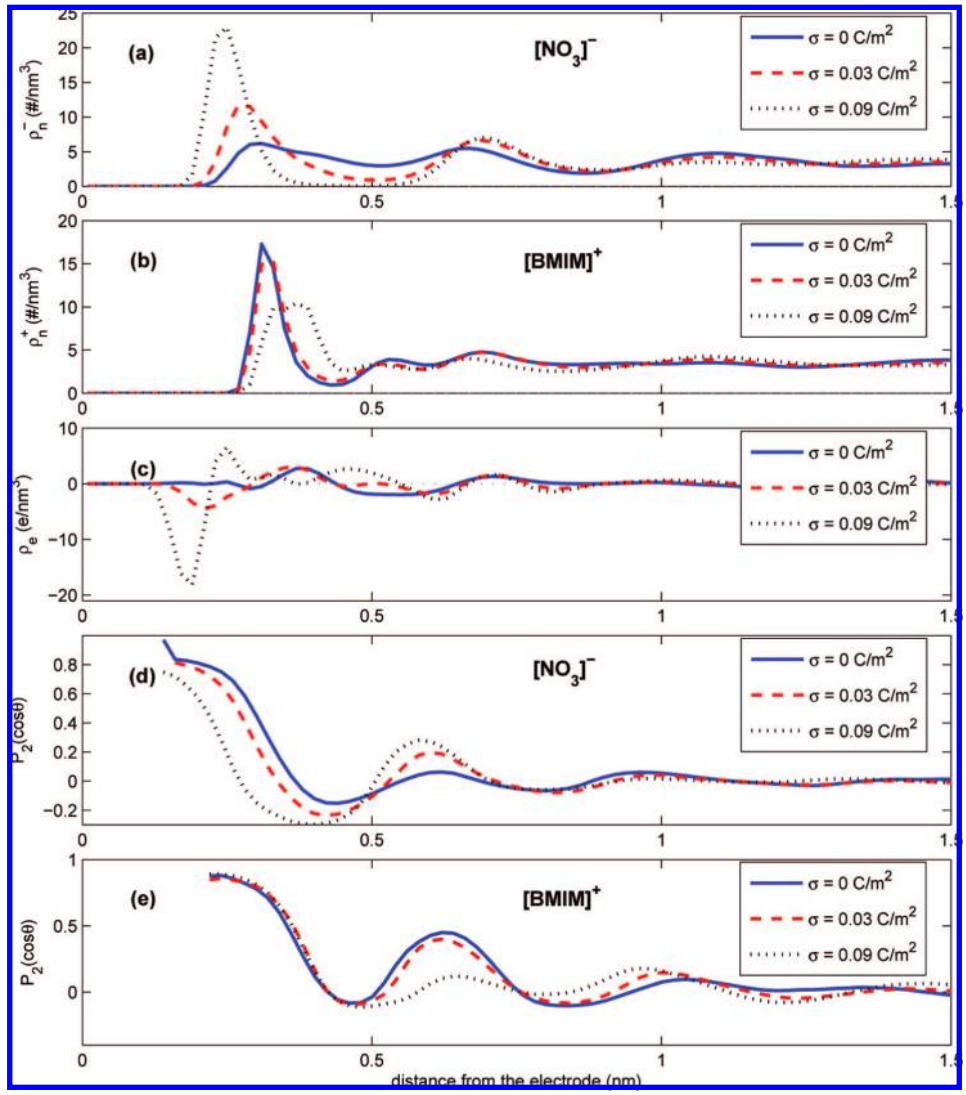

Figure 1. Number density of the $[NO_3]^-$ (panel a) and $[BMIM]^+$ (panel b) ions near neutral and negatively charged electrodes. (c) Space charge density profiles near the electrodes. (d, e) Orientational order parameter $P_2(\cos\theta)$ of $[NO_3]^-$ (panel d) and $[BMIM]^+$ (panel e) ions near neutral and negatively charged electrodes.

$P_2(\cos\theta)$ near the electrode for the $[NO_3]^-$ and $[BMIM]^+$ ions, respectively. We observe that at a position very close to the electrode, both $[BMIM]^+$ and $[NO_3]^-$ ions orient nearly parallel to the electrode and become more random as they move away from the electrode. However, the orientational ordering disappears only at a position about 1.1 nm from the electrode.

Figure 2a and b shows the number density profiles of the $[BMIM]^+$ and $[NO_3]^-$ ions near negatively charged electrodes. We observe that the $[BMIM]^+$ ion exhibits a distinct peak at a position 0.31 nm from the electrode, and the height of the peak increases weakly as σ becomes more negative. Unlike the $[NO_3]^-$ ions near positively charged electrodes, the $[BMIM]^+$ layer near negative electrodes can be delineated even at very low charge densities. We also observe that as σ becomes more negative, although the first density peak of the $[NO_3]^-$ ion moves away from the electrode, its magnitude increases notably. At $\sigma = -0.09$ C/m^2, the density of the $[NO_3]^-$ ion at its first peak ($z = 0.59$ nm) is 2.4 times of that in the bulk. Such a phenomenon is not only rarely observed in aqueous electrolytes and high-temperature molten salts but also difficult to explain by the recent EDL models developed for ILs. The orientational ordering of the $[BMIM]^+$ and $[NO_3]^-$ ions shows a feature similar to that near positively charge electrodes and is not shown.

Discussion. Although the above results are obtained for a specific type of IL, they can provide useful insights into the generic picture of the EDLs in ILs.

First of all, the liquid nature of ILs and short-range interactions play a key role in shaping the EDL structure. The "ionic" nature of the ILs (i.e., IL molecules carry net charges) is clearly important in determining the long-range electrostatic interactions and, thus, the EDL structure. But we also note that, as far as the molecular structure at the IL-electrode interface is concerned, ILs are also "liquids", and the interfacial structure of the ILs near electrodes (i.e., the structure of the EDLs) should at least partly observe the generic theory for the molecular structure at liquid−solid interfaces. Specifically, the short-range (electrostatic or nonelectrostatic) IL−IL and IL−electrode interactions (or, equivalently, the short-range ion−ion and ion-electrode correlations) play an important role in determining the structure of the ILs near the electrode.[23] We expect that the effects of these interactions and correlations on the EDL structure to be particularly significant at low surface charge densities and should remain important at high surface charge densities. These expectations are confirmed by the results shown in Figures 1 and 2. First, as shown in Figure 1 a and b, near neutral electrodes, ILs exhibit significant density oscillation that is

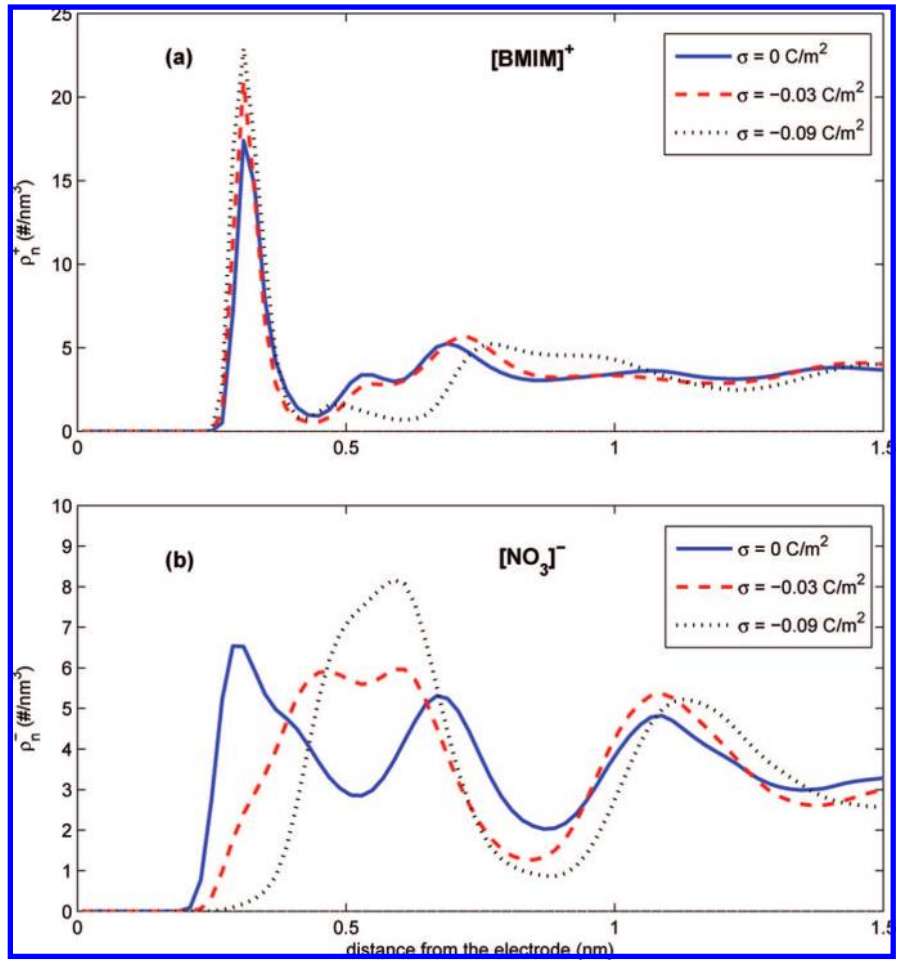

Figure 2. Number density of $[BMIM]^+$ (panel a) and $[NO_3]^-$ (panel b) ions near neutral and negatively charged electrodes.

characteristic of the interfacial liquid structure,[23] and such oscillation penetrates about 1.0 nm into the ILs. Since the electrode is electrically neutral, such rich structure is induced mainly by the short-range interactions and correlations. At $\sigma = \pm 0.03$ C/m^2, these density oscillations persist, and the shape of the space charge density profile near the electrode remains similar to that near neutral electrodes (see Figure 1c). This suggests that the EDL structure is still strongly affected by the short-range IL−IL and IL−electrode interactions. Similar conclusions have also been reached for the EDLs in high-temperature molten salts.[24−27] However, in high-temperature molten salts, the density oscillation penetrates much deeper (about 2 nm) into the bulk salts.[24−26] Such a difference is most likely caused by the fact that the short-range correlation between the smaller ions in molten salts is much stronger as compared to that between bulky ions in ILs, and thus, the structuring of liquids caused by such short-range correlations extends deeper into the bulk liquids for molten salts. In addition, as indicated by the high density peak at $z = 0.31$ nm (see Figure 1b), $[BMIM]^+$ ions are adsorbed persistently on the electrodes, even when they are positively charged. Such a phenomenon appears to be consistent with the experimental observation in refs 28 and 29 and has also been observed in the MD simulation of [DMIM][Cl] near structureless electrodes.[30] Such adsorption, although unfavorable from a long-range electrostatic interactions perspective, is favorable, considering the van der Waals interactions between the cation and the electrode. In fact, for a cation ring oriented parallel to the electrode, the nonelectrostatic interaction energy between the ring and the electrode is -2.42 k_BT (k_B is the Boltzmann constant, and $T = 360$ K) at a ring−electrode separation of 0.31 nm, which can induce significant $[BMIM]^+$ adsorption on the electrode. Finally, as shown in Figure 2, the peak of the $[NO_3]^-$ density profile near negatively charged electrodes increases as σ becomes more negative. Such a phenomenon is caused by the strong interactions between the $[BMIM]^+$ and $[NO_3]^-$ ions. Specifically, as the σ becomes more negative, more $[BMIM]^+$ ions are adsorbed onto the electrode, and they bring more anions toward the electrode.

Second, the charge delocalization can play an important role in determining the EDL structure. Unlike in simple electrolytes, the charge of the ions in ILs is distributed among many atoms. Since the characteristic length of such delocalization is on the order of 3−5 Å, which is comparable to the thickness of the EDLs in ILs, the charge delocalization can potentially have profound impact on the long-range electrostatic interactions in EDLs. Specifically, the mean electrostatic force acting on an ion centered at position r, which affects heavily the EDL structure, depends not only on the electrical field at position r but also on the electrical field in the vicinity of r and the ion orientation. To appreciate this, we consider the mean electrostatic force acting on a $[BMIM]^+$ ion located at position 0.33 nm from an electrode with $\sigma = -0.09$ C/m^2 (the position of this ion is marked by the vertical dash line in Figure 3a). The total mean force acting on the $[BMIM]^+$ ion located here can be computed by $f_{tot} = -k_BT\, d \ln \rho(z)/dz = 25.5 k_BT$/nm, where k_B is the Boltzmann constant and T is the temperature. Figure 3b shows the mean electrical field near the electrode (the calculation of the mean electrical potential and field will be discussed in the section EDL Capaticance.). On the basis of Figure

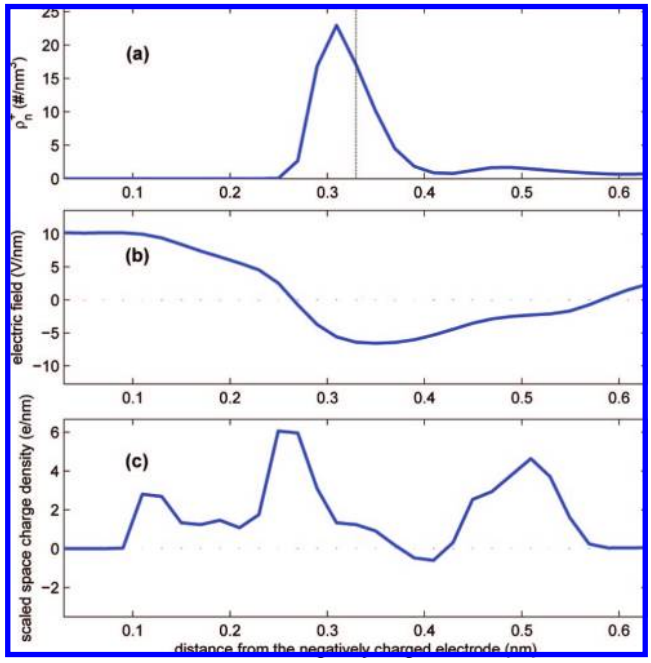

Figure 3. (a) Number density profiles of the $[BMIM]^+$ ions near the negatively charged electrode with a surface charge density of -0.09 C/m^2. (b) Mean electrical field near the electrode. (c) The space charge density due to the presence of a $[BMIM]^+$ ion centered at a position 0.34 nm away from the electrode (this position is indicated by a vertical dash line in panel a).

3b, a naive calculation without considering the charge delocalization indicates that the mean electrostatic force acting on the $[BMIM]^+$ ion centered at $z = 0.33$ nm is $-207.7\ k_BT$/nm, which differs qualitatively from the total mean force computed above. Figure 3c shows the distribution of the space charge density due to the $[BMIM]^+$ ion centered at $z = 0.33$ nm, and we observe that the charge of this ion is distributed in the broad region of 0.1−0.58 nm from the channel wall. Using the mean electrical field in Figure 3b and the space charge density profile in Figure 3c, the mean electrostatic force acting on the $[BMIM]^+$ ion is found to be 19.6 k_BT/nm, which is close to the total mean force calculated above. Although a firm conclusion on the effects of charge delocalization on EDL structure cannot yet be drawn without further detailed study, the above results do suggest that charge delocalization can play an important role in affecting the mean electrostatic force acting on the ions in ILs and, thus, the ion distribution in EDL.

These insights point to important directions for improving the theoretical models for the EDLs in ILs. For example, it is important to account for the effects of short-range IL−IL and IL−electrode interactions and charge delocalization on the ion distribution inside the EDL, which are neglected in most EDL models. These insights also open up new avenues for controlling the microstructure and macroscopic properties of the EDLs in ILs. For example, since the short-range IL−electrode interactions depend strongly on the surface chemistry of the electrode, it is possible to manipulate the structure and properties of the EDL (e.g., capacitance) by tuning the surface functionalization of the electrodes.

B. EDL Capacitance. ***Capacitance Calculation and Results.*** For each case studied, the electrical potential distribution, $\phi(z)$, inside the channel is computed by using[31,32]

$$\phi(z) = \frac{\sigma}{\varepsilon_0} z - \frac{1}{\varepsilon_0}\int_0^z (z - z')\,\rho_e(z')\,dz' \qquad (1)$$

where ε_0 and $\rho_e(z)$ are the vacuum permittivity and space charge density inside the channel, respectively. Figure 4 shows the electrical potential distribution when the surface charge density on the two opposite channel walls is ± 0.03 C/m^2. Similar to that in high-temperature molten salts, significant oscillation of the electrical potential is observed near the electrified surface.[24,26]

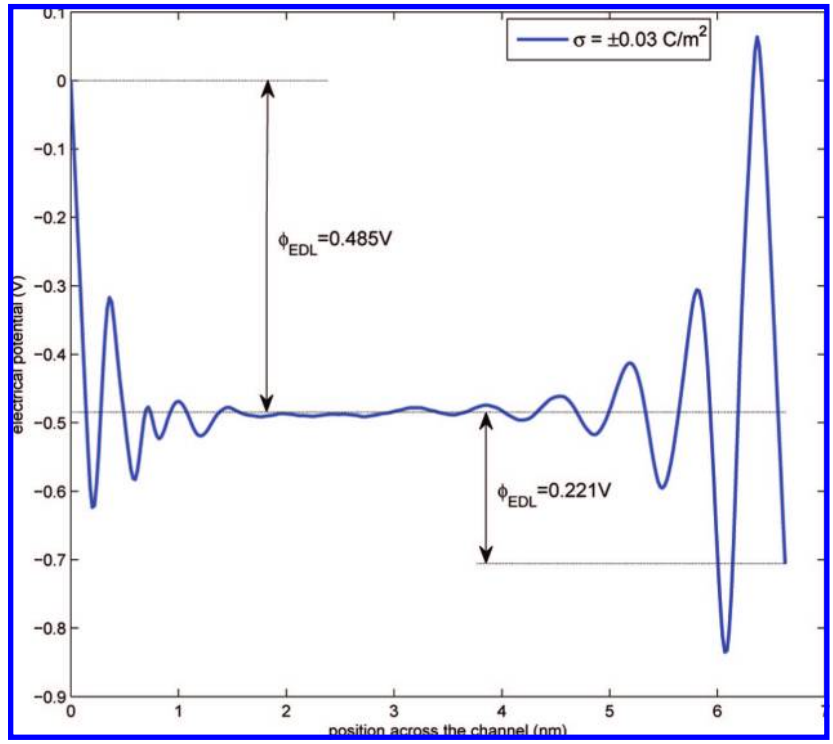

Figure 4. Distribution of the electrical potential across the channel (channel wall charge density: ± 0.03 C/m^2). Because the electrical potential in the central portion of the channel is flat, the potential drop across the EDLs, $\Delta\phi_{EDL}$, near the upper and lower channel walls can be evaluated from the electrical potential profile shown here.

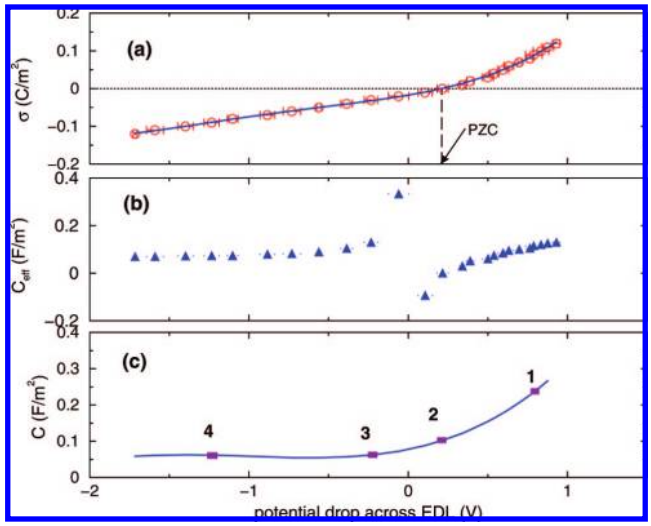

Figure 5. (a) Correlation between the electrode charge density and the electrical potential drop across the EDLs at the interface of [BMIM][NO_3] and planar electrodes. (b) Correlation between the effective EDL capacitance, $C_{eff} = \sigma/\phi_{EDL}$, and the electrical potential drop across the EDL for systems studied in this paper. (c) Correlation between the EDL differential capacitance, $C = d\sigma/d\phi_{EDL}$, and the electrical potential drop across the EDL.

Since the electrical potential in the central portion of the channel is constant, the potential drop across the EDLs, ϕ_{EDL}, near each of the channel walls was then identified as shown in Figure 4. Using this procedure, ϕ_{EDL} for EDLs near channel walls with a surface charge density ranging from -0.12 to $+0.12$ C/m^2 was obtained. Figure 5a shows the computed $\phi_{EDL} - \sigma$ correlation.

In the literature, the EDL capacitance has been computed in two different ways. An effective EDL capacitance, C_{eff}, can computed by using $C_{eff} = \sigma/\phi_{EDL}$,[24] and a differential EDL capacitance, C, can be computed by using $C = d\sigma/d\phi_{EDL}$. Here, we computed the EDL capacitance using both approaches. When computing the differential capacitance, the $\phi_{EDL} - \sigma$ correlation was first fitted to a fourth-order polynomial, and the differential capacitance was then obtained by analytically differentiating the polynomial. Figure 5b and c shows the dependence of the effective capacitance, C_{eff}, and the differential capacitance, C, on the potential drop across the EDL, respectively. The effective capacitance, C_{eff}, shown in Figure 5b shows a trend similar to that reported for the EDL in high-temperature molten salts; that is, C_{eff} exhibits a discontinuity near the potential of zero charge (PZC) and decreases as the potential increases from PZC and increases as the potential decreases from the PZC.[24] We note that the negative capacitance near PZC is caused by the definition of C_{eff} and should not be confused with the negative differential capacitance discussed in the literature.[33] Since the differential capacitance has more detailed information on the charge storage capability of the EDL, we will focus on the differential capacitance in the rest of our discussion. An examination of the capacitance−potential correlation shown in Figure 5c shows that (1) at positive electrode polarization, the EDL capacitance increases sharply as the electrode potential becomes more positive, and (2) at negative electrode polarization, the EDL capacitance varies only weakly as the electrode potential becomes more negative. These trends agree very well with those observed experimentally at the interface of [EMI][BF_4] and mercury electrodes,[14] although they differ qualitatively from the bell-shaped and camel-like $C-V$ curves obtained at the interface of [BMIM][Cl] and glassy carbon electrodes.[12] Below, we explore the molecular origins of trends of the capacitance−potential ($C-V$) correlation shown in Figure 5c. To this end, we first establish the connection between the structure and the capacitance of an EDL and then investigate the dependence of the differential capacitance on positive and negative electrode polarizations.

Relation between EDL Structure and Capacitance. The differential capacitance is a macroscopic manifest of how the structure of the EDL near an electrode responds to a change of the electrode potential or surface charge density. To obtain a mathematical model for this, we consider the EDL near an open planar electrode with a surface charge density of σ (see Figure 6). The potential distribution inside the EDL observes the Poisson equation

$$\frac{d^2\phi}{dy^2} = -\frac{\rho_e(y)}{\varepsilon_0} \tag{2}$$

If the potential ϕ at distance L from the electrode, where the space charge density is zero, is set to zero, then

$$\phi(y) = -\frac{1}{\varepsilon_0}\int_0^y \int_0^{y'} \rho_e(x)\, dx\, dy' \tag{3}$$

Using integration by parts, eq 3 is transformed to

$$\phi(y) = -\frac{1}{\varepsilon_0}\int_0^y (y - y')\, \rho_e(y')\, dy' \tag{4}$$

Therefore, the potential drop across the EDL is

$$\phi_{EDL} = \phi(L) - \phi(0) = -\frac{1}{\varepsilon_0}\int_0^L (L - y')\, \rho_e(y')\, dy' \tag{5}$$

If the charge density of the electrode changes by a small amount, $\Delta\sigma$, there will be a corresponding change in the space charge density (thereafter denoted as $\Delta\rho_e(y)$) inside the EDL. Because of the linearity of eqs 2 and 5 with respect to the space charge density, the change in the potential drop across EDL as the electrode surface charge density increases from σ to $\sigma + \Delta\sigma$ ($\Delta\phi_{EDL}$) is

$$\Delta\phi_{EDL} = \phi_{EDL}|_{\sigma+\Delta\sigma} - \phi_{EDL}|_{\sigma} = -\frac{1}{\varepsilon_0}\int_0^L (L - y')\, \Delta\rho_e(y')\, dy' \tag{6}$$

Since $C = (\Delta\sigma/\Delta\phi_{EDL})$ and $\Delta\sigma = -\int_0^L \Delta\rho_e(y)\, dy$,

$$C = \frac{\varepsilon_0}{\int_0^L (L - y)(-\Delta\rho_e(y))\, dy \Big/ \int_0^L (-\Delta\rho_e(y))\, dy} \tag{7}$$

Since $L - y$ is the distance between point y and the electrode surface (see Figure 6), eq 7 can be transformed to the z-coordinate system as

$$C = \frac{\varepsilon_0}{\int_0^L z(-\Delta\rho_e(z))\, dz \Big/ \int_0^L (-\Delta\rho_e(z))\, dz} = \frac{\varepsilon_0}{d_{eff}} \tag{8}$$

Equation 8 provides the connection between the differential capacitance of an EDL and how its microstructure changes as the charge density on the electrode changes. Interestingly, it shows that the differential capacitance of an EDL can always be casted into a form similar to the capacitance of the EDLs observing the Helmholtz model. However, there are distinct differences between this general model and the Helmholtz model. Specifically, in the Helmholtz model, $C = \varepsilon/d$, where ε is the permittivity inside the EDL and d is the distance between the counterion layer and the electrode. In the present model, which is more useful when the EDL is explicitly resolved at the atomistic scale, the vacuum permittivity is used, and d_{eff} is

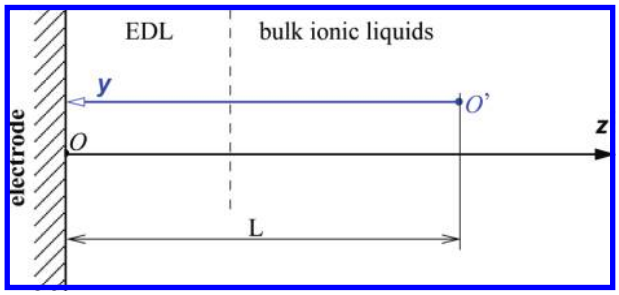

Figure 6. Two coordinate systems used to derive the relation between the structure and capacitance of an EDL. The first, *y*-coordinate system has its origin in the bulk ionic liquids, where the space charge density is zero. The second, *z*-coordinate system has its origin at the electrode surface.

an effective separation. Mathematically, d_{eff} can be interpreted as the mean separation between points in EDL and the electrode weighted by the variation of space charge density ($-\Delta\rho_e(z)$) at these points when a small charge is added to the electrode. Therefore, in the present model, the capacitance is not *directly* controlled by the separation between the counterion and the electrode, as in the Helmholtz model, but is directly controlled by how the *variation of space charge density* ($\Delta\rho_e(z)$) is distributed as a change in electrode charge density is introduced. For a given $\Delta\sigma > 0$, the $\Delta\rho_e(z)$ will be predominately negative in order to screen the increased electrode charge. In principle, the EDL capacitance can only be determined by using the distribution of $\Delta\rho_e(z)$. However, typically, the capacitance will be higher if the increased electrode charge $\Delta\sigma$ is screened at a shorter distance from the electrode by $\Delta\rho_e(z)$, since the integral $\int_0^L -z\Delta\rho_e(z)\,dz$ in eq 8 tends to be smaller in such a case.

Capacitance at Positive Electrode Polarization. To understand the molecular mechanisms of the trends of the $C-V$ correlation shown in Figure 5c, we selected two representative points on the $C-V$ curve (point 1, with $\phi_{EDL} = 0.80$ V and $\sigma = 0.09$ C/m^2, and point 2, with $\phi_{EDL} = 0.21$ V and $\sigma = 0$ C/m^2) and investigate why the capacitance at point 1 is higher than that at point 2. To this end, we study the response of the EDL structure at these points as the electrode charge densities σ increase. We will first show how and why the change of the ion number density is different at these operating points when the same small $\Delta\sigma$ is introduced. We next show how the different change in ion number density leads to different changes in space charge density and, thus, different capacitance at these two operating points.

Figure 7a1 and a2 shows the variation of $[NO_3]^-$ density ($\Delta\rho_n^-$) at operating points 1 and 2 when σ increases by 0.01 C/m^2. Both figures show similar trend in $\Delta\rho_n^-$: a distinct peak is observed next to the electrode, followed by alternating valleys and peaks; that is, as the electrode charge density increases, a large number of $[NO_3]^-$ ions are added to the region next to the electrode; meanwhile, some $[NO_3]^-$ ions are added/removed in other regions. The appearance of alternating peaks and valleys beyond the first $\Delta\rho_n^-$ peak are caused by the correlation between $[NO_3]^-$ ions. For example, the first $\Delta\rho_n^-$ valley appears because as more $[NO_3]^-$ ions accumulate in the first $[NO_3]^-$ layer near the electrode, their repulsive interactions with the $[NO_3]^-$ ions located at positions near the first $[NO_3]^-$ layer tend to deplete $[NO_3]^-$ ions at these positions. Such a depletion process is observed clearly by comparing the $[NO_3]^-$ ion density in the region 0.30 nm $< z <$ 0.55 nm at different electrode charge densities (see Figure 1a). A key difference between the $\Delta\rho_n^-$ profiles at operating points 1 and 2 is that the first $\Delta\rho_n^-$ peak is closer to the electrode at operating point 1. This is mainly due to the stronger $[NO_3]^-$−electrode interaction at operating point 1. The accumulation of $[NO_3]^-$ ions in the region next to the electrode is favored by their electrostatic interactions with the electrode but is also hindered by the "desolvation effects"; that is, as a $[NO_3]^-$ ion moves toward the electrode, it becomes less "solvated" by the $[BMIM]^+$ ions due to geometrical confinement. We note that the importance of such "desolvation effects" has long been recognized in the study of high-temperature molten salts.[24] At point 1, where σ is higher, the first factor dominates, and thus, the added ions accumulate at nearly the closest approach to the electrode. At point 2, where σ is small, the second factor becomes important. Thus, ions accumulate at positions further away from the electrode. To further quantify how the $[NO_3]^-$ ions are added into the EDL, we integrate the $\Delta\rho_n^-$ profile from the electrode toward the bulk IL. The results are shown in Figure 7c1 and c2. At operating point 1, we observe that the $[NO_3]^-$ ion added to the first $\Delta\rho_n^-$ peak and valley (0.2 nm $< z <$ 0.60 nm) is nearly 100% of the total amount of the $[NO_3]^-$ ion added into the EDL. However, at operating point 2, the $[NO_3]^-$ ion added to the first $\Delta\rho_n^-$ peak and valley (0.2 nm $< z <$ 0.61 nm) is close to zero; that is, effectively, no $[NO_3]^-$ ion is added into the region 0.2 nm $< z <$ 0.61 nm. Such a difference is mainly caused by the desolvation effect, which significantly hinders the accumulation of $[NO_3]^-$ ion within a distance of ~0.68 nm from the electrode surface. Specifically, on the basis of the $[BMIM]^+$−$[NO_3]^-$ pair correlation function, the solvated radius of $[NO_3]^-$ ion is ~0.68 nm.[18] Therefore, a $[NO_3]^-$ ion will start to lose its "solvation" ions when it approaches the electrode surface closer than 0.68 nm. Figure 7b1 and b2 shows the variation of $[BMIM]^+$ density ($\Delta\rho_n^+$) at points 1 and 2 when σ increases by 0.01 C/m^2. Both parts of the figure show a $\Delta\rho_n^+$ valley near the electrode, followed by alternating $\Delta\rho_n^+$ peaks and valleys. Integrations of the $\Delta\rho_n^+$ profiles are shown in Figure 7c1 and c2. Comparison of the integration of $\Delta\rho_n^+$ and $\Delta\rho_n^-$ profiles indicates that, for both operating points 1 and 2, the change in the number of $[NO_3]^-$ ions inside the EDL is more than 3.75 times larger than that of the $[BMIM]^+$ ion. This suggests that the response of the EDL structure to a change in the electrode charge is dominated by the $[NO_3]^-$ ions.

Figure 7a1, a2 and b1, b2 also shows the changes of space charge density ($\Delta\rho_e^-$ and $\Delta\rho_e^+$) associated with the change in $[NO_3]^-$ and $[BMIM]^+$ ion density when the electrode charge increases by 0.01 C/m^2 at points 1 and 2. We observe that although the overall trends of $\Delta\rho_e$ profiles are similar to that of the $\Delta\rho_n$ profiles, these profiles do not match exactly. This is caused by the charge delocalization of the IL ions. Specifically, $\Delta\rho_e$ at a position z depends on the $\Delta\rho_n$ in its vicinity and the orientation of IL ions. For example, the positive $\Delta\rho_e^-$ in 0.2 nm $< z <$ 0.29 nm is mainly a result of the positive $\Delta\rho_n^-$ in 0.17 nm $< z <$ 0.25 nm and the fact that positively charged nitrogen atoms of the $[NO_3]^-$ ions centered in this region are located in 0.2 nm $< z <$ 0.29 nm.

Since the total variation of space charge density is $\Delta\rho_e = \Delta\rho_e^+ + \Delta\rho_e^-$, using the $\Delta\rho_e^-$ and $\Delta\rho_e^+$ obtained above and eq 8, one can prove mathematically that the EDL capacitance at point 1 is higher than that at point 2. However, to obtain a more intuitive, albeit qualitative, understanding of how these different $\Delta\rho_e$ profiles lead to different capacitance, we adopt a different approach here. As mentioned earlier, the EDL capacitance is typically higher if the increased electrode charge, $\Delta\sigma$, is screened at a shorter distance from the electrode by $\Delta\rho_e(z)$. To quantify this screening, we integrate the $\Delta\rho_e$ profiles from the electrode surface toward the bulk ILs. The results are shown in Figure

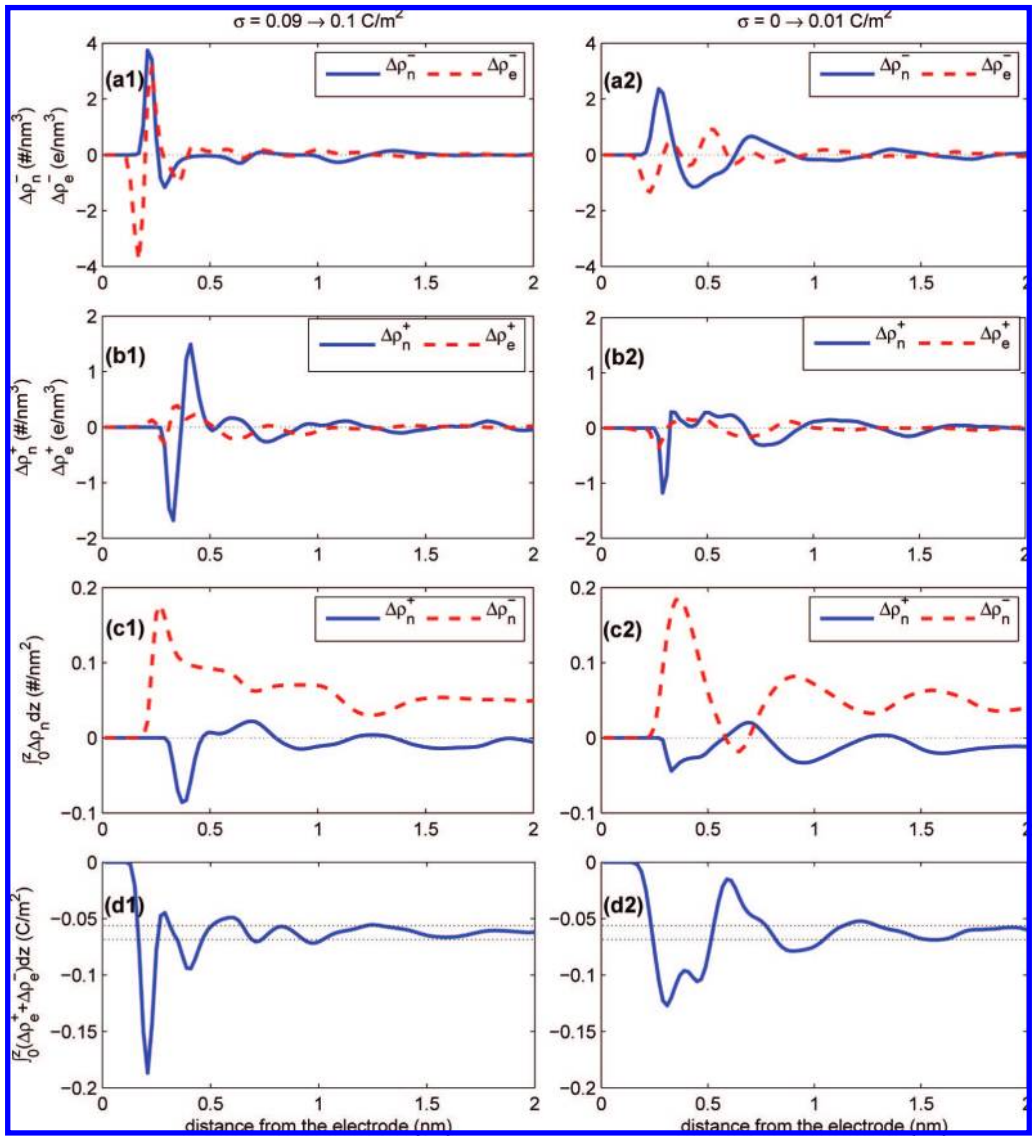

Figure 7. Response of the EDL structure at operating points 1 and 2 (see Figure 5c) as the electrode charge density increases by 0.01 C/m^2. The left panels are results for point 1, and the right panels are results for point 2. (a1, a2) Variation of the number density of $[NO_3]^-$ ion ($\Delta\rho_n^-$) and the associated change in space charge density ($\Delta\rho_e^-$). (b1, b2) Variation of the number density of $[BMIM]^+$ ion ($\Delta\rho_n^+$) and the associated change in space charge density ($\Delta\rho_e^+$). (c1, c2) Integration of $\Delta\rho_n^-$ and $\Delta\rho_n^+$ from the electrode surface toward the bulk IL. (d1, d2) Integration of $\Delta\rho_e = \Delta\rho_e^+ + \Delta\rho_e^-$ from the electrode surface toward the bulk IL. The two dash lines correspond to the 90% and 110% screening of the increased surface charge density by the ions.

7d1 and d2. Figure 7d1 and d2 shows that the increased electrode charge ($\Delta\sigma = 0.01$ C/m$^2 = 0.0625$ e/nm^2) is essentially screened at a position about 0.65 and 1.0 nm from the electrode at point 1 and point 2, respectively, thus confirming that the capacitance at point 1 is higher than that at point 2. To trace the molecular origins of the different screening of $\Delta\sigma$ (and, thus, the capacitance) at these points, we first note that the screening of $\Delta\sigma$ is dominated by the addition of $[NO_3]^-$ ions into the EDL at both points 1 and 2. By correlating Figure 7 part d1 with parts c1 and a1, we next note that the effective screening of $\Delta\sigma$ at a small distance from the electrode at point 1 is mainly due to the closeness of the first $\Delta\rho_n^-$ peak to the electrode and the fact that nearly all $[NO_3]^-$ ions necessary to screen the increased surface charge are added to the region $z < 0.60$ nm. In contrast, at point 2, the effective screening of $\Delta\sigma$ is achieved at a larger distance from the electrode because the first $\Delta\rho_n^-$ peak is farther away from the electrode, and essentially, no additional $[NO_3]^-$ ion is added to the region $z < 0.61$ nm as the electrode charge density increases from 0.09 to 0.10 C/m^2.

To summarize, the response of EDL structure at positive electrode polarization to a change of electrode charge is dominated by the addition of $[NO_3]^-$ ions into the EDL. The addition of $[NO_3]^-$ ions into the EDL is controlled by both electrode−ion interactions and the desolvation effects. At high surface charge density (polarization), the electrode−ion interactions dominate, and many $[NO_3]^-$ ions are introduced at their closest approach to the electrode, and almost all $[NO_3]^-$ ions needed to screen the increased surface charge are introduced within 0.60 nm from the electrode, thus leading to a high capacitance. At low surface charge, the desolvation effects dominate, and the net number of $[NO_3]^-$ ions added to the region $z < 0.61$ nm, in which $[NO_3]^-$ ion experiences desolvation, is nearly zero. As such, a low capacitance is observed.

Capacitance at Negative Electrode Polarization. Here, we select two representative points on the $C-V$ curve shown in Figure 5c, point 3 with $\phi_{EDL} = -0.20$ V and $\sigma = -0.03$ C/m^2 and point 4 with $\phi_{EDL} = -1.24$ V and $\sigma = -0.09$ C/m^2. We investigate why the capacitance at these points is similar by

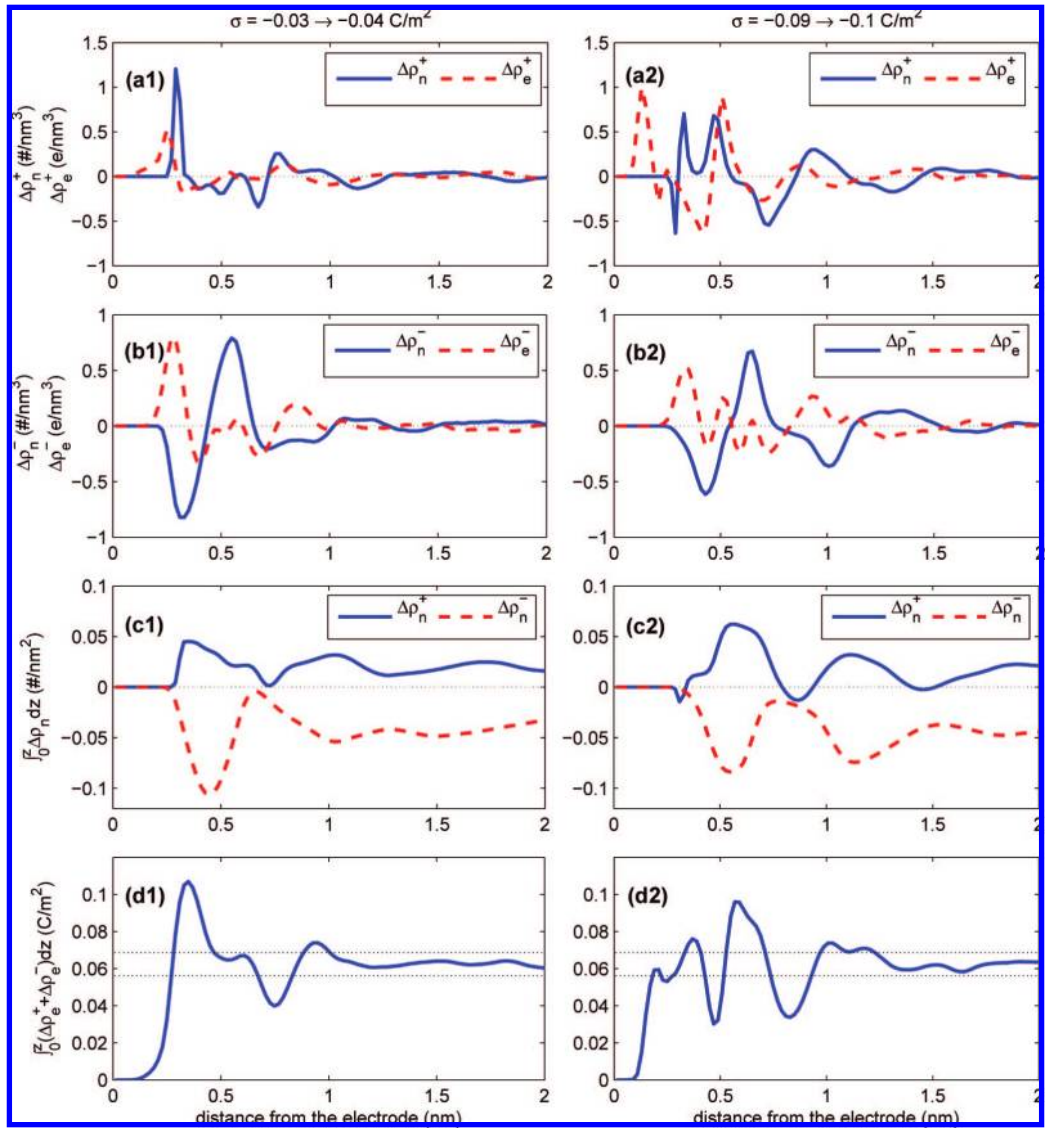

Figure 8. Response of the EDL structure at operating points 3 and 4 (see Figure 5c) as the electrode charge density decreases by 0.01 C/m^2. The left panels are results for point 3, and the right panels are results for point 4. (a1, a2) Variation of the number density of $[BMIM]^+$ ion ($\Delta\rho_n^+$) and the associated change in space charge density ($\Delta\rho_e^+$). (b1, b2) Variation of the number density of $[NO_3]^-$ ion ($\Delta\rho_n^-$) and the associated change in space charge density ($\Delta\rho_e^-$) (c1, c2) Integration of $\Delta\rho_n^-$ and $\Delta\rho_n^+$ from the electrode surface toward the bulk IL. (d1, d2) Integration of $\Delta\rho_e = \Delta\rho_e^+ + \Delta\rho_e^-$ from the electrode surface toward the bulk IL. The two dash lines correspond to the 90% and 110% screening of the increased surface charge density by the ions.

studying the response of the EDL structure to a change in the electrode charge.

Figure 8a1 and a2 shows the variation of $[BMIM]^+$ density ($\Delta\rho_n^+$) at operating points 3 and 4 when σ decreases by 0.01 C/m^2. Both parts of the figure show trends similar to those observed for the $[NO_3]^-$ ion in Figure 7a1 and a2. Figure 8b1 and b2 shows the variation of $[NO_3]^-$ density at operating points 3 and 4 under the same conditions. Both parts show a significant valley (i.e., removal of ions) in the region 0.2 nm $\lesssim z \lesssim$ 0.5 nm because of the increased electrostatic repulsion by the electrode. This is followed by a peak (0.50 nm $\lesssim z \lesssim$ 0.7 nm), which is caused by the increase of $[BMIM]^+$ ion near the electrode and the strong $[BMIM]^+-[NO_3]^-$ correlations. This peak induces another valley in the region (0.70 nm $\lesssim z \lesssim$ 1.1 nm) due to the correlations between $[NO_3]^-$ ions. To quantify how many ions are added to (or removed from) the EDL as the electrode charge decreases by $\Delta\sigma$, we again integrate the $\Delta\rho_n$ profiles from the electrode toward the bulk IL; the results are shown in Figure 8c1 and c2. We observe that, at both operating points, (1) the total number of $[NO_3]^-$ ions removed from the EDL is much larger than the number of $[BMIM]^+$ ions added into the EDL, and (2) the total number of $[NO_3]^-$ ions removed in the first $\Delta\rho_n^-$ peak and valley is only a small fraction of the total number of $[NO_3]^-$ ions removed from the EDL. Observation 1 suggests that the response of EDL structure to a change in electrode charge is dominated by the $[NO_3]^-$ ions, even at negative electrode polarization, which is different from the situations in aqueous electrolytes, in which the response of the EDL structure to a change in the electrode charge is typically dominated by the counterions. This phenomenon is caused by (1) unlike the EDLs in aqueous electrolyte, in which the co-ion density is low, there are a large number of co-ions inside the EDLs in ILs available for removal, and (2) a large number of $[BMIM]^+$ ions pack closely near the electrode at zero charge (see Figure 8a1). Therefore, as the electrode becomes more negatively charged, it is much more difficult to insert a bulky $[BMIM]^+$ ion into the densely packed EDL than removing a smaller $[NO_3]^-$ ion. Observation 2 is mainly caused by the strong correlations between $[NO_3]^-$ and $[BMIM]^+$ ions. Specifically, the removal of $[NO_3]^-$ ions from the region $z <$ 0.7 nm

is hindered by the attractive forces exerted on these ions by the large number of $[BMIM]^+$ ions accumulated near the electrode. Such attractive forces do not depend strongly on the electrode charge density since the $[BMIM]^+$ ion accumulation near the electrode varies weakly with the electrode charge (see Figure 2a).

Figure 8a1, a2 and b1, b2 also shows the changes of space charge density ($\Delta\rho_e^+$ and $\Delta\rho_e^-$) associated with the change in $[BMIM]^+$ and $[NO_3]^-$ ion density when the electrode charge decreases by 0.01 C/m^2 at points 3 and 4. Integration of these profiles from the electrode surface toward the bulk ILs provides information on how the increased negative charge ($\Delta\sigma$) is screened by the variation of the space charge density ($\Delta\rho_e = \Delta\rho_e^+ + \Delta\rho_e^-$) inside the EDL. The results are shown in Figure 8d1 and d2. We observe that the $\Delta\sigma$ is effectively screened at a position $\approx$1.05 nm from the electrode at both operating points, which suggests that the capacitance at these two operating points is similar. By correlating Figure 8, parts d1, d2 with parts b1, b2 and a1, a2, we note that the effective screening of $\Delta\sigma$ at such a relatively large distance from the electrode originates from the fact that very few $[NO_3]^-$ ion are removed from the region $z < 0.7$ nm due to the strong attractive force exerted on these ions by the $[BMIM]^+$ ions adsorbed on the electrode.

To summarize, the response of the EDL structure at negative electrode polarization to a decrease in the electrode charge is dominated by the removal of $[NO_3]^-$ ions from the EDL. Because the removal of $[NO_3]^-$ ions from the region near the electrode is hindered by their attractive interactions with the large number of $[BMIM]^+$ ions accumulated near the electrode, $[NO_3]^-$ ions are mainly removed from the region away from the electrode. Consequently, the capacitance is small. Since the aforementioned attractive interactions depend weakly on the electrode charge, the capacitance is insensitive to the electrode charge density.

Discussion. Although the differential capacitance of an EDL is one of its most important macroscopic properties, its current understanding is limited. The above results provide new insights into this problem and point to possible directions to improve the current EDL models. First of all, the EDL capacitance in ILs does not depend simply on the closest approach between the counterion and electrode, as is often assumed in the literature. For example, the closest approach between the $[NO_3]^-$ ion and the electrode reduces by 17% as the electrode potential increases from 0.21 to 0.80 V, but the capacitance increases by 140%. In addition, the results near a negatively polarized electrode suggest that the co-ion also plays a critical role in determining the EDL capacitance. Second, the cation−anion correlations and the significant adsorption of cations on the electrode at zero electrode charge can strongly affect the EDL capacitance. It will be worthwhile to systematically study these effects and incorporate them into theoretical EDL models. An exciting possibility with these effects is that they may explain the very diverse trends of capacitance−potential ($C-V$) curves observed experimentally. For example, since the adsorption of ions on electrodes (and thus, the capacitance) depends strongly on their surface chemistry and the surface chemistry of electrodes made of even the same materials can differ significantly due to different fabrication details, it is possible that the diverse $C-V$ correlations observed by different research groups originate from the different surface chemistries of the electrodes used by them.

Another important property of the EDL is the potential of zero charge of the electrode. On the basiss of the data shown in Figure 5a and c, it was determined that the PZC of the present electrode is 0.21 V, whereas the potential at which the EDL capacitance reaches minimum is −0.5 V. This differs from the typical expectation that the PZC coincides with the minimum of the $C-V$ curve. However, since not all physical processes (e.g., the specific adsorption of ions on the electrodes) are accounted for in the present simulations, further studies are needed to clarify the relation between the PZC and the minimum of $C-V$ curves in ionic liquids.

IV. Conclusion

The structure and capacitance of the EDLs at the interface of an ionic liquid [BMIM][NO_3] and planar electrodes were studied at various electrode surface charge densities by using classical molecular dynamics simulations. The complex shape of the ions and their delocalized charge distribution are modeled explicitly, and the nonelectrostatic interactions between ions and the electrodes are also accounted for.

The study of EDL structure near electrodes with different surface charge densities indicates that a Helmholtz-like interfacial counterion layer exists when the electrode charge density is negative or strongly positive but becomes not well-defined when the electrode charge density is weakly positive. However, regardless of the presence of a distinct Helmholtz layer, the charge separation (i.e., nonzero space charge locally) and orientational ordering of the ions persist to a depth up to 1.1 nm into the bulk ILs. These results support the composite EDL structure proposed in the literature.[8,9] Further analysis of these results suggests that structure of the EDL is affected strongly by the liquid nature of the IL and the short-range ion-electrode and ion−ion interactions, especially at low electrode charge densities. In addition, the charge delocalization is found to affect the mean force experienced by the bulky ions near the electrode and, thus, can play an important role in shaping the EDL structure.

For the specific system studied here, the EDL capacitance is nearly constant under negative electrode polarization but increases dramatically with the electrode potential under positive electrode polarization. The capacitance is interpreted as a response of the EDL structure to a change in the electrode charge. It is found that the $[NO_3]^-$ ion dominates the response of EDL structure to the change in the electrode charge under both positive and negative electrode polarization. Detailed analysis shows that the cation−anion correlations and the strong adsorption of $[BMIM]^+$ ions on the electrode are responsible for the capacitance−potential correlation observed here.

Acknowledgment. R.Q. gratefully acknowledges help from Drs. Soares, Micaelo, and de Andrade during the initial stage of this study. The authors thank the Clemson-CCIT office and the Center for Nanoscale Materials (CNM) at Argonne National Laboratory for providing computer time. Use of the Center for Nanoscale Materials was supported by the U.S. Department of Energy, Office of Science, Office of Basic Energy Sciences, under Contract No. DE-AC02-06CH11357.

References and Notes

(1) Kosmulski, M.; Tendaj, B. *Przem. Chem.* **2001**, *80*, 280.
(2) McEwen, A.; Ngo, H.; LeCompte, K.; Goldman, J. *J. Electrochem. Soc.* **1999**, *146*, 1687.
(3) de Andrade, J.; Boes, E. S.; Stassen, H. *J. Phys. Chem. B* **2002**, *106*, 13344.
(4) Ohno, H., *Electrochemical Aspects of Ionic Liquids*; John Wiley and Sons, Inc.: New York, 2005.
(5) Balducci, A.; Dugas, R.; Taberna, P.; Simon, P.; Plee, D.; Mastragostino, M.; Passerini, S. *J. Power Sources* **2007**, *165*, 922.
(6) Ue, M.; Takeda, M.; Toriumi, A.; Kominato, A.; Hagiwara, R.; Ito, Y. *J. Electrochem. Soc.* **2003**, *150*, A499.

(7) Largeot, C.; Portet, C.; Chmiola, J.; Taberna, P.; Gogotsi, Y.; Simon, P. *J. Am. Chem. Soc.* **2008**, *130*, 2730.
(8) Kornyshev, A. *J. Phys. Chem. B* **2007**, *111*, 5545.
(9) Oldham, K. *J. Electroanal. Chem.* **2008**, *613*, 131.
(10) Baldelli, S. *Acc. Chem. Res.* **2008**, *41*, 421.
(11) Baldelli, S. *J. Phys. Chem. B* **2005**, *109*, 13049.
(12) Lockett, V.; Sedev, R.; Ralston, J.; Horne, M.; Rodopoulos, T. *J. Phys. Chem. C* **2008**, *112*, 7486.
(13) Alam, M.; Islam, M.; Okajima, T.; Ohsaka, T. *Electrochem. Commun.* **2007**, *9*, 2370.
(14) Alam, M.; Islam, M.; Okajima, T.; Ohsaka, T. *J. Phys. Chem. C* **2007**, *111*, 18326.
(15) Pinilla, C.; Popolo, M. D.; Kohanoff, J.; Lynden-Bell, R. *J. Phys. Chem. B* **2007**, *111*, 4877.
(16) Fedorov, M. V.; Kornyshev, A. A. *J. Phys. Chem. B* **2008**, *112*, 11868–11872.
(17) *Gromacs User Manual*, version 3.0; Nijenborgh 4, 9747 AG; Groningen, The Netherlands, 2001; Internet: http://www.gromacs.org.
(18) Micaelo, N. M.; Baptista, A. M.; Soares, C. M. *J. Phys. Chem. B* **2006**, *110*, 14444.
(19) Lindahl, E.; Hess, B.; van der Spoel, D. *J. Mol. Model.* **2001**, *7*, 306.
(20) Darden, T.; York, D.; Pedersen, L. *J. Chem. Phys. van der Spoel* **1993**, *98*, 10089.
(21) Yeh, I.; Berkowitz, M. *J. Chem. Phys.* **1999**, *111*, 3155.
(22) Hess, B.; Bekker, H.; Berendsen, H.; Fraaije, J. *J. Comput. Chem.* **1997**, *18*, 1463.
(23) Israelachvili, J., *Intermolecular and Surface Forces*; Academic Press: New York, 1992.
(24) Reed, S. K.; Lanning, O. J.; Madden, P. A. *J. Chem. Phys.* **2007**, *126*, 084704.
(25) Esnouf, R. M.; Grout, P. J. *Philos. Mag. A* **1988**, *58*, 27.
(26) Lanning, O. J.; Madden, P. A. *J. Phys. Chem. B* **2004**, *108*, 11069.
(27) Heyes, D. M.; Clarke, J. H. R. *J. Chem. Soc., Faraday Trans. 2* **1981**, *77*, 1089.
(28) Fukushima, T.; Kosaka, A.; Ishimura, Y.; Yamamoto, T.; Takigawa, T.; Ishii, N.; Aida, T. *Science* **2003**, *300*, 2072.
(29) Fukushima, T.; Aida, T. *Chem.—Eur. J.* **2007**, *13*, 5048.
(30) Pinilla, C.; Popolo, M. D.; Lynden-Bell, R.; Kohanoff, J. *J. Phys. Chem. B* **2005**, *109*, 17922.
(31) Spohr, E. *Electrochim. Acta* **1999**, *44*, 1697.
(32) Sachs, J. N.; Crozier, P. S.; Woolf, T. B. *J. Chem. Phys.* **2004**, *121*, 10847.
(33) Luo, H.; Yu, M. Y. *Phys. Scr.* **2006**, *74*, 670.

JP809900W